Biochemistry

 Volume 33, Number 37 September 20, 1994

Articles

Three-Dimensional Structure in Solution of Neurotoxin III from the Sea Anemone *Anemonia sulcata*

Nick Manoleras

School of Biochemistry and Molecular Genetics, University of New South Wales, Kensington 2033, Australia

Raymond S. Norton*

NMR Laboratory, Biomolecular Research Institute, 381 Royal Parade, Parkville 3052, Australia

Received April 25, 1994; Revised Manuscript Received July 8, 1994®

ABSTRACT: The three-dimensional structure in aqueous solution of the 27-residue polypeptide neurotoxin *Anemonia sulcata* toxin III (ATX III) has been determined from ^{1}H NMR data. As ATX III self-associates in the millimolar concentration range, causing a marked concentration dependence for the chemical shifts of several residues [Norton, R. S., Cross, K., Braach-Maksvytis, V., & Wachter, E. (1993) *Biochem. J.* 293, 545–551], it was necessary to record NOESY spectra over a range of concentrations in order to eliminate any intermolecular interactions from the NOE restraint set. The pairings of the six half-cystine residues were also unknown and had to be determined (as 3–17, 4–11, and 6–22) from preliminary structure calculations performed using both upper bound distance restraints from NOESY data and a substantial number of lower bound restraints inferred from the absence of NOESY cross-peaks. Final structures were determined, using the program X-PLOR, from interproton distance restraints inferred from NOEs, backbone and side chain dihedral angle restraints from spin–spin coupling measurements, and a smaller number of lower bound restraints. Stereospecific assignments for 11 β-methylene pairs were also included. The final set of 28 structures had an average pairwise RMS difference of 1.32 Å over the backbone heavy atoms (N, C$^\alpha$, and C) and 2.18 Å over all heavy atoms. For the well-defined region encompassing residues 3–22, the corresponding values were 0.62 and 1.28 Å, respectively. ATX III adopts a compact structure containing four reverse turns (a distorted type I β-turn at residues 6–9, a type I β-turn at residues 8–11, and inverse γ-turns at residues 12–14 and 15–17) and two other chain reversals, but no regular α-helix or β-sheet. Several of the residues most affected by aggregation are located on the surface of the molecule, forming a hydrophobic patch which may constitute part of the sodium channel binding surface. Possible relationships between the structure of ATX III and those of other sea anemone toxins that interact with the same site on the voltage-gated sodium channel are considered.

The sea anemone *Anemonia sulcata* produces a variety of polypeptide toxins, among which are several that target the voltage-gated sodium channel of excitable tissue (Beress, 1982). The neurotoxins ATX I,[1] ATX II, and ATX V (Beress, 1979, 1982) from this species have molecular masses of about 5000 Da and belong to a group classified as "long" toxins (Kem, 1988; Norton, 1991). On the basis of amino acid sequence homology and immunological cross-reactivity, these long toxins have been differentiated further into type 1, from the genera *Anemonia* and *Anthopleura*, and type 2, from the

* To whom correspondence should be addressed. Fax: +61-3-903 9655. Phone: +61-3-903 9650. Email: ray@mel.dbe.csiro.au.

® Abstract published in *Advance ACS Abstracts*, August 15, 1994.

[1] Abbreviations: ATX I–V, *Anemonia sulcata* toxins I–V; PaTx, *Parasicyonis actinostoloides* toxin; Sh I, *Stichodactyla helianthus* neurotoxin I; 1D, one-dimensional; 2D, two-dimensional; NMR, nuclear magnetic resonance; NOE, nuclear Overhauser enhancement; NOESY, 2D NOE spectroscopy; DQF-COSY, double quantum filtered 2D correlated spectroscopy; RMS, root mean square.

0006-2960/94/0433-11051$04.50/0

genera *Heteractis* and *Stichodactyla* (Kem, 1988). A smaller number of "short" toxins have also been isolated. ATX III, also from *A. sulcata*, has 27 residues and 3 disulfide bonds (Beress et al., 1975), while ATX IV is identical with ATX III except that it lacks the C-terminal Lys and Val residues (Beress, 1979, 1982), and may in fact be a cleavage product of ATX III generated during extraction. The only other member of this group currently known is PaTx from *Parasicyonis actinostoloides* (Nishida et al., 1985). There is definite amino acid sequence similarity between ATX III and PaTx, and they can be aligned such that 16 residues are identical (Norton, 1991). There is, however, very little similarity between these molecules and the long polypeptide toxins.

The biological activity of ATX III is very similar to that of the long sea anemone toxins in that it binds to the voltage-gated sodium channel and decreases the rate of channel inactivation (Warashina et al., 1988; Norton, 1991). It is likely, furthermore, that their binding sites on the sodium channel (Catterall, 1988) are similar, if not identical, and that there is overlap between the anemone toxin binding site and those for the scorpion α-toxins (Catterall & Beress, 1978) and the anti-hypertensive proteins BDS I and II, also from *A. sulcata* (Llewellyn & Norton, 1991). Mapping this binding site is of interest not only in enhancing our knowledge of the structure and function of the sodium channel but also because at least some of the anemone toxins that bind there are potent cardiac stimulants with therapeutically beneficial properties (Norton, 1981; Renaud et al., 1986). It is expected that knowledge of both the binding site and the binding determinants on the various polypeptides that interact with it will provide a valuable lead in the design of new ligands with the favorable cardiac stimulatory properties of the anemone polypeptides. As the smallest polypeptide known so far to bind to this site, ATX III is thus of special interest. In this paper, we describe its three-dimensional structure in aqueous solution, determined on the basis of ^{1}H NMR data. The structure is then compared with those of the long type 1 toxins AP-A (Torda et al., 1988; Pallaghy, Scanlon, Monks, and Norton, unpublished results) and ATX Ia (Widmer et al., 1989) and the type 2 toxin Sh I (Fogh et al., 1990; Wilcox et al., 1993).

In principle, solving the structure of a polypeptide the size of ATX III from ^{1}H NMR data should be straightforward, taking into account that it has three disulfide bonds which should serve to restrict the global fold. There were, however, two factors that complicated the structure determination in this case. The first was that ATX III aggregates at the millimolar concentrations needed to acquire 2D NMR spectra (Norton et al., 1993). It was therefore necessary to record NOESY spectra over a range of concentrations in order to identify and eliminate any intermolecular NOEs. The second problem was that the disulfide pairings were unknown and that three of the cysteines were close to one another in the sequence, at positions 3, 4, and 6. Structure calculations were therefore carried out without disulfide connectivities made, and the correct pairings were chosen on the basis of half-cystine C^β to C^β distances.

MATERIALS AND METHODS

Materials. The sample of ATX III was supplied by Dr. Laszlo Beress, Institute of Toxicology, University of Kiel, Germany. ^2H_2O, ^2HCl, and NaO^2H were obtained from Cambridge Isotope Laboratories, Woburn, MA.

NMR Spectroscopy. ^{1}H NMR spectra were recorded on Bruker AM-500 (University of New South Wales) and AMX-500 and -600 (Biomolecular Research Institute) spectrometers. All 2D spectra were recorded in the phase-sensitive mode using the time-proportional phase incrementation method (Marion & Wüthrich, 1983). Solvent suppression was achieved by selective, low-power irradiation of the water resonance during the relaxation delay, which was typically 2.0 s, and for NOESY spectra also during the mixing time. NMR data used for structure determination were acquired at 500 MHz on a 5 mM sample of ATX III in 90% H_2O/10% ^2H_2O or ^2H_2O at pH 2.5–2.7 and a temperature of 27 °C. Homonuclear 2D NOESY (Jeener et al., 1979; Macura et al., 1980) were recorded with mixing times of 100–250 ms in 90% H_2O/10% ^2H_2O and 50 and 200 ms in ^2H_2O. Stereospecific assignments and side chain torsion angle constraints, as well as additional distance restraints, were obtained from DQF-COSY (Rance et al., 1983), complementary E-COSY (Griesinger et al., 1987), and two NOESY spectra with mixing times of 50 and 200 ms recorded on a sample of ATX III in ^2H_2O. Typically, spectra were acquired with 220–500 t_1 increments, 64–96 scans per increment, and 2048–4096 data points. To examine the effects of ATX III concentration on chemical shifts and NOEs, NOESY spectra were acquired at 600 MHz on ATX III in ^2H_2O at concentrations of 5, 1, and 0.2 mM. The mixing time was 200 ms, and the numbers of scans per t_1 increment were 64, 128, and 256, respectively.

Spectra were processed on Silicon Graphics IRIS 4D/20 or 4D/70 workstations using FELIX version 1.1 (Hare Research Inc., Bothell, WA). For most spectra, a phase-shifted (30–90°) sine-squared window function was applied prior to Fourier transformation. For the NOESY spectra used to measure cross-peak volumes for distance restraints, a window function was applied that had a value of 1 for points 1–1024 followed by a 90° shifted sine-squared window function over points 1025–2048. Final matrix sizes were generally 2048 × 2048 real points although additional zero-filling was used for the complementary E-COSY and DQF-COSY to give final matrix sizes of 4096 × 4096 and a digital resolution in F_2 of 1.42 Hz/point. Base-line correction of the rows using an in-house program bfx and t_1 noise suppression (Manoleras & Norton, 1992) were applied to each matrix.

Structural Restraints. NOESY cross-peaks were integrated using FELIX to obtain volume lists from the 250 ms mixing time spectrum in H_2O and the 200 ms mixing time spectrum in ^2H_2O. Peaks from the upper side of the diagonal were used except where peaks from the lower side were better resolved. The volumes of cross-peaks from degenerate methylene protons were divided by a factor 2, and all cross-peaks involving the methyl groups were divided by 3. Peak volumes in each matrix were calibrated using an average value of the volumes of eight well-resolved geminal $C^\beta H$ cross-peaks, measured from both sides of the diagonal and assigned a distance of 1.79 Å. Two different sets of structure calculations were performed, with slightly different distance corrections used in each case. To determine the disulfide pairings, structure calculations were performed in DSPACE version 4.1 (Hare Research Inc.), and NOESY cross-peak volumes were divided by a factor of 3 before being converted to upper bound distance restraints. This had the effect of adding about 0.4 Å to the upper bound restraints corresponding to strong NOE cross-peaks and about 0.8 Å to the restraints corresponding to weak NOEs. The final structures were calculated using X-PLOR (Brünger, 1992), for which volumes were converted directly to distances, corrections of 0.5 and 1.0 Å being added to distance restraints involving backbone protons only and at least one side chain proton, respectively.

Backbone dihedral angle restraints were derived from $^3J_{HNC^\alpha H}$ coupling constants measured from 1D spectra as follows: −120° for $^3J_{HNC^\alpha H} > 8$ Hz and −60° for $^3J_{HNC^\alpha H} < 5$ Hz (Pardi et al., 1984). Deviations from these angles varied depending on the value of the coupling constant, the minimum deviation being 30°. Backbone dihedral restraints were not applied for $^3J_{HNC^\alpha H}$ values between 5 and 8 Hz. $^3J_{C^\alpha HC^\beta H}$ coupling constants were measured from either complementary E-COSY or DQF-COSY spectra. To account for inaccuracies caused by large line widths in splittings measured from the DQF-COSY spectrum (Neuhaus et al., 1985), a dispersive line shape fitting program, COUPLING.ERIK, was used, similar to that of Smith et al. (1991). This program uses estimates of the line width at half-height and the apparent coupling, and then attempts a number of simulations using Lorentzian lines to best match the observed cross-peak pattern. These coupling constants, together with $d_{\alpha\beta}(i,i)$ and $d_{N\beta}(i,i)$ NOEs from short mixing time NOESY experiments (50 ms in ^2H_2O and 100 ms in H_2O), were used to determine if side chains could be placed in one of the staggered side chain rotamer conformations ($\chi^1 = 60$, 180, and −60°) and to make stereospecific assignments (Wagner et al., 1987; Hyberts et al., 1987). Stereospecific assignments for proline $C^\beta H$ resonances were based on the relative intensities of the $C^\alpha H$–$C^\beta H$ NOE cross-peaks in the 50 ms NOESY in ^2H_2O (Clore et al., 1986). Extension of stereospecific assignments to the proline $C^\gamma H$ and $C^\delta H$ resonances was not possible because of the degeneracy or near-degeneracy of the $C^\gamma H$ resonances (Norton et al., 1993). χ^1 torsion angles were constrained to values of 60, 180, or −60° as appropriate, with minimum deviations of 30°.

Negative Restraints from NOESY Spectra. Just as the presence of a NOESY cross-peak implies a short distance (generally <5 Å) between a proton pair, the absence of a cross-peak, or "non-NOE", can imply a large distance and constitute a useful structural restraint (de Vlieg et al., 1986; Wilcox et al., 1993). In this work, a program, designated NONNOE, has been written to extract lower bound constraints from NOESY spectra in a conservative fashion that takes account of factors such as internal motion and spectral artifacts which might adversely affect measured NOE intensities.

This program operates on 2D matrices in the FELIX format and measures a volume for *every* possible pairwise interaction, that is, between every pair of protons in the chemical shift assignment list. Volumes over a defined footprint are measured using the expression:

$$V_{ij} = \sum_{i=N-n}^{i=N+n} \sum_{j=M-m}^{j=M+m} |I_{ij}| \qquad (1)$$

where I_{ij} is the intensity of point ij, N and M are the center points of the footprint in F_1 and F_2, respectively, and $2n+1$ and $2m+1$ are the dimensions of the footprint in F_1 and F_2. As it is necessary to ensure that the real volume is not underestimated, the absolute value of every point in the footprint is summed in order to account for spectral artifacts, the presence of which will generally increase the volume measurement. These measured cross-peak volumes are then evaluated to account for other factors that can lead to reduced enhancements (Neuhaus & Williamson, 1989), the most common of which in a diamagnetic protein such as ATX III is internal motion. For this purpose, an NOE retention factor, q_i, is assigned to each resonance i, based on the expression:

$$q_i = \left(\frac{m_{ij}}{1.79}\right)^6 \frac{V_{ij}}{V_{ref}} \qquad (2)$$

V_{ij} is the measured volume for the cross-peak between protons i and j, V_{ref} is the average calibration volume described above to convert NOESY volumes into upper bound distance restraints, and m_{ij} is the minimum possible distance separating protons i and j. Thus, where spectral artifacts, internal motion, or other factors decrease the intensity of a given cross-peak, $q_i < 1$ will be recorded for the contributing protons. Cross-peaks from protons separated by fixed distances, such as geminal protons, were used where possible to derive retention factors, but in other cases intraresidue and sequential distances had to be used because of peak overlap. For a $C^\alpha H$ resonance, for example, the intraresidue $d_{N\alpha}$ cross-peak could be used, with m_{ij} set to the minimum distance of 2.2 Å. This distance can vary from 2.2 to 2.9 Å depending on the backbone ϕ angle (Wüthrich, 1986), so taking the minimum distance is conservative and will at worst define a retention factor lower than necessary. For a few resonances, no suitable intraresidue or sequential cross-peaks could be found, and cross-peaks from longer range interactions had to be used; in these cases, m_{ij} was set to 1.8 Å, leading to low values for the calculated retention factors.

Finally, lower bound restraints (in the range 2.5–4.0 Å) were calculated from

$$l_{ij} = 1.79\left(\frac{q_i q_j V_{ref}}{k_s V_{ij}}\right)^{1/6} \qquad (3)$$

where k_s is a constant that was set to 3 in the present study to provide an adequate margin between l_{ij} and the corresponding upper bound. Where l_{ij} calculated from eq 3 was <2.5 Å, a default lower bound of 1.8 Å was used, while the maximum allowed value for l_{ij} was 4.0 Å. Lower bounds were calculated in this way for all pairwise interactions, regardless of whether or not an upper bound restraint based on an observed NOE was present.

Structure Calculations for Determinations of Disulfide Pairings. These calculations, carried out using DSPACE,[2] were based on upper bound distance restraints derived from NOESY cross-peak volumes and lower bound restraints from non-NOEs. DSPACE uses as the driving force for structural convergence a penalty function which is a weighted sum of the squares of the violations of bond lengths and angles, rigid distances, van der Waals interactions, and hydrogen bonds, as well as the experimentally derived restraints. The weighting for each type of violation was set to 1 except for the Lennard–Jones potential, which was not used. Floating chirality (Weber et al., 1988) was used at all prochiral carbons having methylene protons with nondegenerate chemical shifts. Both embedded and randomized structures were used as starting structures. Refinement began with variable target function conjugate gradient minimization on the local structure, starting at the N-terminus and minimizing residues 1–4, and then shifting one residue and minimizing residues 2–5 and continuing until the C-terminus was reached. Conjugate gradient minimization was then carried out over the entire molecule. Simulated annealing was performed in four dimensions and then in three dimensions and was followed by variable target function conjugate gradient minimization over the entire molecule. Only structures that had a total penalty function less than a defined allowable maximum were retained. To overcome a problem associated with ω angle violations, all accepted structures were subjected to a routine to correct ω angles that deviated unacceptably from 180° (Pallaghy et al., 1993).

[2] These calculations were later repeated using X-PLOR and the restraint set used to generate the final structures, but with the disulfide connectivities excluded. The same pattern of disulfide bond connectivities emerged as for the preliminary DSPACE calculations.

Calculation of Final Structures. The final set of structures was calculated using X-PLOR, version 3.1. Until the final stage of refinement, the covalent geometry for the disulfide bridges 3–17, 4–11, and 6–22 was replaced by distance restraints of 2.02 ± 0.1 Å between the sulfur atoms. Embedded starting structures were calculated using metric matrix distance geometry. These structures were then regularized by simulated annealing using the all-hydrogen distance geometry parameter and topology files in X-PLOR. Initially, 1000 annealing steps at 2000 K were used, minimizing on bond, van der Waals, and NOE energies and then including angles, chirality, and planarity energy terms. This was followed by 1000 cooling cycle steps during which the van der Waals radii were gradually increased. Structures were then refined using simulated annealing from a temperature of 2000 K to 100 K using 2000 cooling steps. The NOE distance restraints between the sulfur atoms were removed and replaced by covalent geometry for the three disulfide bonds, and the refinement stage was then repeated. Finally, 2000 steps of Powell conjugate gradient minimization were used. Final structures were selected based on the criteria of no NOE restraint violations greater than 0.5 Å, no dihedral angle violations greater than 5°, RMS differences for bond lengths of less than 0.01 Å, and RMS differences for bond angles of less than 2°. The 28 final structures and the NMR restraints used in their determination have been deposited with the Brookhaven Protein Data Bank (Accession No. 1ANS).

Structural characteristics were analyzed using the program SSTRUC, based on the methods of Kabsch and Sander (1983). Surface areas were calculated in Insight II (Biosym Technologies, San Diego, CA) from Connolly surfaces generated with a 1.4 Å probe radius.

RESULTS

Concentration Dependence. The chemical shifts and line widths of a number of resonances in ATX III are markedly concentration dependent over the millimolar concentration range needed to acquire 2D NMR spectra (Norton et al., 1993), and preliminary analytical ultracentrifugation results indicate that association extends at least to the formation of trimers at a concentration of 5 mM.[3] It was therefore necessary to establish that the NOE set used as the basis for structure determination did not contain contributions from intermolecular interactions.

This was assessed by recording NOESY spectra at ATX III concentrations of 5, 1, and 0.2 mM in ^2H_2O. Preliminary analytical ultracentrifugation results indicate that at the lowest of these concentrations the protein is largely monomeric,[3] although the signal-to-noise ratio in this spectrum was too low to afford a useful set of structural constraints. Inspection of the chemical shifts at these three concentrations, however, showed that significant concentration-dependent shifts occurred for only six residues, *viz.*, Pro5, Tyr7, Trp8, Cys11, Pro12, and Trp13 (Figure 1). One or more resonances from each of these residues changed chemical shift by at least 0.05 ppm between 5 and 1 mM, whereas for all other residues the maximum change was 0.02 ppm, the average being 0.006 ppm. Between 1 and 0.2 mM, resonances from these six residues shifted by a further 0.01–0.03 ppm. The structures described below show that these residues lie close together on the molecular surface, forming a hydrophobic patch. The presence of three aromatic rings in this region is no doubt partly responsible for the sensitivity of the chemical shifts of these residues to aggregation, and our observations do not rule out the possibility of contributions from other regions of the molecule to the aggregation surface. Indeed, the greater propensity for aggregation at pH 6 than at pH 2 (Norton et al., 1993) implies that one of the two carboxylate groups in the molecule contributes to aggregation. Nevertheless, the fact that the six residues noted above do display concentration-dependent chemical shifts suggests that intermolecular NOEs, if they are present at all, should be observed for at least some of these residues.

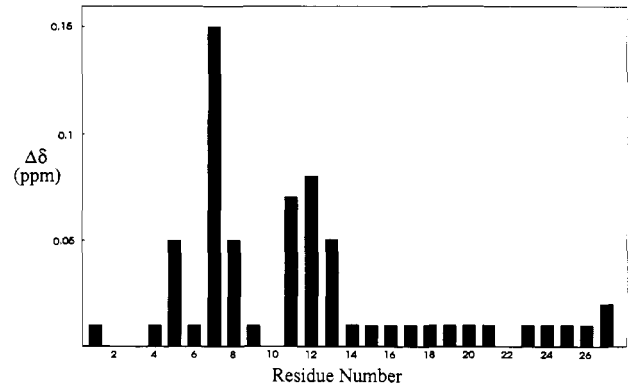

FIGURE 1: Changes in chemical shift between NOESY spectra recorded at ATX III concentrations of 5 and 1 mM in ^2H_2O at pH 2.5–2.7. The maximum change in chemical shift for any resonance in a given residue is plotted. For Arg1, Ser2, Tyr7, Trp8, Trp13, Glu16, Pro19, and Ser23, some resonances could not be assigned in one or both spectra. The large downfield shift of the C(2,6)H resonance of Tyr7 between 5 and 1 mM places it downfield of the C(3,5)H resonance at the lower concentrations.

The NOESY spectra at different concentrations were assessed by choosing a group of 80 cross-peaks that was clearly visible at both 1 and 5 mM. Because of the lower signal-to-noise ratio at 1 mM, this group consisted mainly of cross-peaks having volumes consistent with a proton separation of 3 Å or less, but it included 6 medium-range ($i - j < 5$) and 16 long-range ($i - j \geq 5$) NOEs, 8 of which were from the 6 residues identified above. The volumes of each of the 80 peaks in the 5 mM spectrum were then divided by the corresponding values from the 1 mM spectrum, yielding a range of factors from 2.2 to 11.4 with a mean (±SD) at the expected value of 5.0 ± 2.0. For the eight NOEs involving the residues with chemical shifts most affected by aggregation, the mean was 5.8 ± 1.8 and the range 3.3–9.1. The smaller peaks were mainly responsible for the significant deviations from the average, and, importantly, there was no consistent pattern in the distribution of deviations which might point to the involvement in intermolecular interactions of particular residues. The poor signal-to-noise ratio in the 0.2 mM spectrum made it impractical to extend this approach to this concentration. Some weak cross-peaks were present in this spectrum that were consistent with expected long-range NOEs between ring protons of Trp8 and Trp13, but their intensities were too low for distances to be inferred. However, given that the major changes in chemical shifts and line widths occurred between 5 and 1 mM [see also Figure 1 of Norton et al. (1993)] and that the relative NOE intensities at 1 mM were similar to those at 5 mM, it appears that intermolecular interactions do not contribute significantly to the measured NOE intensities. Further evidence in support of this comes from an assessment of NOE violations in the final structures (see below). None of the structures had violations greater than 0.5 Å, and even when values between 0.3 and 0.5 Å were considered, violations of NOEs to the six residues strongly affected by aggregation did not occur with significantly higher frequency than those to other residues.

[3] G. J. Howlett, unpublished results.

Determining Disulfide Pairings. Various NMR-based methods are available for determining the correct pairings of half-cystine residues in the absence of chemical data. Initially, the observation of NOEs between protons of half-cystine residues was used (Williamson et al., 1985), but in many cases this does not give unequivocal results, especially when there is a large number of disulfides in the molecule. More recently, structure calculations have been carried out without disulfides formed, and the appropriate connectivities have been chosen on the basis of S^{γ}–S^{γ} distances (Johnson & Sugg, 1992; Cooke et al., 1992), C^{β}–C^{β} distances (Klaus et al., 1993), or visual inspection (Adler et al., 1993). Structures can also be calculated with different sets of disulfide connectivities and evaluated for agreement with the set of NMR constraints (Heitz et al., 1989; Metzler et al., 1992; Cooke et al., 1992; Adler et al., 1993). Klaus et al. (1993) have shown that only $C_i^{\alpha}H/C_j^{\beta}H$ and $C_i^{\beta}H/C_j^{\beta}H$ NOEs have a positive predictive value for a disulfide connectivity between half-cystines *i* and *j*. For ATX III, it has been determined previously from such NOEs that the 6–22 disulfide pairing was very likely but that the pairings for the other two bonds were ambiguous because of the adjacent half-cystine residues at positions 3 and 4 in the sequence (Norton et al., 1993). In this work, therefore, we have used a method similar to that of Klaus et al. (1993), where the C^{β}/C^{β} distances between all half-cystines are analyzed. The C^{β}/C^{β} distances were used in preference to distances involving the sulfur atoms because C^{β} atoms have a reduced degree of freedom relative to the sulfurs.

DSPACE was used to calculate families of structures in which no restraints, covalent or otherwise, were placed between half-cystines. These families of structures were based on upper bound restraints from NOESY data, 8 backbone dihedral angle restraints (converted into distance restraints), and a set of 4600 lower bound restraints derived as described under Materials and Methods. The inclusion of a large set of lower bound restraints in a situation like this is beneficial as they assist in restricting the conformational space available to the molecule and of course do not contain intermolecular contributions. Lower bound restraints must be used with caution because of the potential of causes other than a large distance between a pair of protons to reduce or eliminate NOEs (de Vlieg et al., 1986; Neuhaus & Williamson, 1989). In our implementation, the effects of spectral artifacts and fast internal motions that might quench enhancements have been addressed by the introduction of a retention factor for each resonance, determined as described under Materials and Methods. Figure 2 summarizes the average retention factors for $C^{\beta}H$ resonances (or $C^{\alpha}H$ resonances in the case of Gly residues) observed in this study. Although high retention factors are determined for residues from more rigid parts of the molecule (see below), low values do not arise only from mobile residues, as other influences such as spectral artifacts may also give rise to low values. Very few NOESY cross-peaks could be found for residues Arg1, Ser2, and Ser23, and these residues are poorly defined in the final structures (see below). Correspondingly, the retention factors for most resonances in these residues are zero or near zero (Figure 2), and no lower bound restraints based on non-NOEs would be used for these residues.

DSPACE was used in these calculations because it incorporates floating chirality (Weber et al., 1988) and could be applied before the full set of stereospecific assignments was available. Furthermore, lower bound restraints could be included in DSPACE calculations without any significant increase in the CPU execution time (Wilcox et al., 1993). In fact, two sets of structure calculations were carried out, one

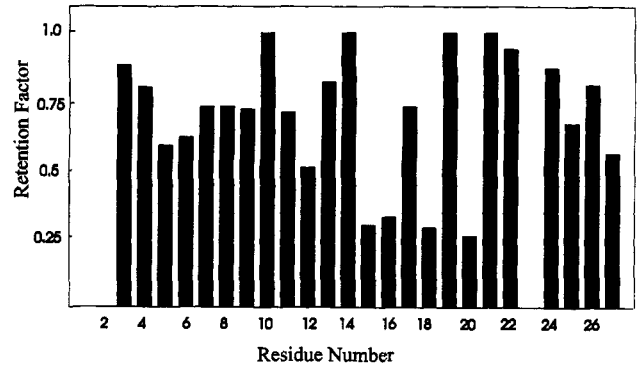

FIGURE 2: NOE retention factors as a function of residue number for $C^{\beta}H$ resonances (or $C^{\alpha}H$ resonances in the case of Gly residues). The derivation of these factors is described under Materials and Methods. Retention factors were calculated using intraresidue $C^{\beta}H$–$C^{\beta}H$ (or $C^{\alpha}H$–$C^{\alpha}H$) cross-peaks, except as follows: $C^{\alpha}H$–$C^{\beta}H$ for residues 8, 12, and 27; $C^{\beta}H$–C(2,6)H for Tyr18; and $C^{\beta}H$–$C^{\gamma}H$ for Glu20. Interresidue (long-range) cross-peaks had to be used for residues 9 and 15, while the absence of clearly defined cross-peaks to the $C^{\beta}H$ resonances of residues 1, 2, and 23 resulted in retention factors of zero for these resonances. Note that retention factors are calculated for individual resonances in each residue and may vary significantly from one proton in a given residue to another.

including all upper bound distance restraints (254 at this stage) and the other with the 42 restraints to the 6 residues Pro5, Tyr7, Trp8, Cys11, Pro12, and Trp13 eliminated in order to avoid possible complications due to intermolecular NOEs. Only NOEs that could be unambiguously assigned and which did not duplicate restraints imposed by the covalent geometrywere used. In both cases, the hydrogen atom bonded to the sulfur was excluded from the cysteine topology file so as not to restrict the space occupied by the sulfur atoms.

On the basis of the lowest overall penalty functions, 18 structures were selected from the set generated using all restraints while 22 were selected from the set that excluded the distance restraints between the residues affected by aggregation. As structures that were not converging were automatically rejected, the overall number of structures that was attempted in each set was not recorded. The C^{β}/C^{β} distances between all possible combinations of Cys residues in these families of structures are shown in Figure 3. Assuming undistorted bond lengths and angles, the distance between these atoms across a disulfide bond ranges from 3.2 to 4.7 Å, as shown in Figure 3. In the family of structures generated with all restraints, it is quite clear that the correct disulfide pairings are 3–17, 4–11, and 6–22, the distances between all other pairs being well outside the acceptable region except for the 3–4 pairing, which is close to the allowed range because of their proximity as sequential residues. Nevertheless, a disulfide link between these adjacent half-cystine residues is unlikely because the requirement that the intervening peptide bond adopt the *cis* conformation (Blake et al., 1994) is not met. Even in the set of structures generated with the exclusion of NOE restraints from residues affected by aggregation, the correct disulfide pairings can be established because the pairings 3–17 and 6–22 fall within the acceptable region, leaving 4–11 as the only possible third pairing.[2]

The family of structures calculated with the exclusion of NOE restraints between the residues affected by aggregation was poorly defined, having an average RMS difference calculated (in DSPACE) over all backbone heavy atoms (N, C^{α}, C) of 1.63 Å, as compared with 1.25 Å for the family calculated using all restraints. As described below, the six residues most affected by aggregation lie close together on the molecular surface, forming a hydrophobic patch. It follows that in the structures calculated without restraints to these

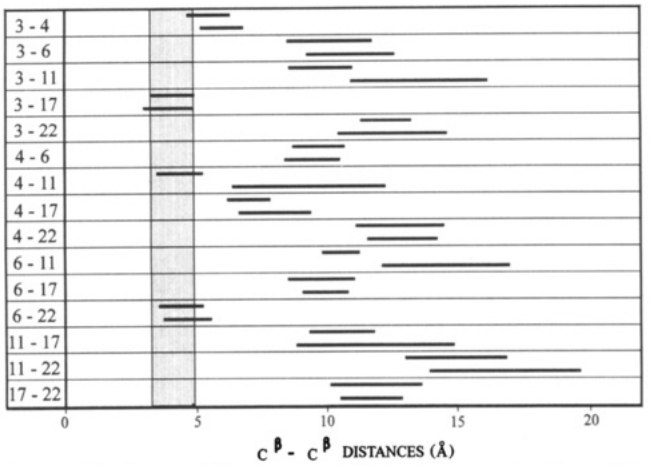

FIGURE 3: Ranges of half-cystine C^{β}–C^{β} distances for all possible disulfide pairings in structures of ATX III calculated without disulfide links. The set of structures corresponding to the top line in each case was generated with a full set of upper bound restraints whereas the set corresponding to the bottom line was generated without NOEs involving the six residues known to be affected by aggregation, *viz.*, Pro5, Tyr7, Trp8, Cys11, Pro12, and Trp13. The shaded region shows the expected range for this distance for disulfide-linked half-cystines.

Table 1: Stereospecific Assignments and χ^1 Angle Constraints for ATX III at pH 2.5 and 27 °C[a]

residue	$C^{\beta}H$ chemical shift (ppm) and stereospecific assignment[b]		χ^1
Cys3	3.09 β3	2.92 β2	–60°
Cys4	3.41 β3	2.43 β2	–60°
Pro5	2.13 β2	0.66 β3	
Cys6	2.12 β2	1.72 β3	+60°
Tyr7	3.47 β2	2.93 β3	+60°
Cys11	2.09 β3	0.14 β2	+60°
Pro12	2.40 β2	2.13 β3	
Cys17	3.36 β3	2.78 β2	–60°
Pro19	2.28 β2	2.01 β3	
Cys22	3.29 β3	2.98 β2	–60°
Pro25	2.27 β2	1.82 β3	

[a] A complete listing of chemical shifts and assignments is given in Norton et al. (1993). [b] β2 corresponds to *Pro*(*S*) and β3 to *Pro*(*R*).

residues, this region of the molecule was poorly defined. As this region includes Cys11, all disulfide pairing combinations involving Cys11 display a wide range of distances in Figure 3. Nevertheless, the correct pairing of 4 to 11 (as required by the well-defined pairings of the other four half-cystines) still has the shortest average distance of any of the possible pairings involving Cys11, indicating that the local structure determined in the absence of these NOEs is consistent with that in their presence.

Structure Determination. Structures were calculated using the disulfide pairings 3–17, 4–11, and 6–22, as determined above, and assuming that all observed NOEs arose from intramolecular interactions. On the basis of $^3J_{HNC^{\alpha}H}$ coupling constants, the ϕ angles of residues 13, 15, 17, 20, and 27 were constrained to –120° and those of 4, 16, and 22 to –60°. Stereospecific assignments and χ^1 angle constraints, obtained as described under Materials and Methods, are summarized in Table 1. Initial structures were calculated using 254 upper bound distance restraints from NOESY cross-peaks that could be unambiguously assigned. With the benefit of structural feedback, in-house software was used (Wilcox et al., 1993) to check all NOE assignments and assign additional NOE corss-peaks that previously could not be assigned unambiguously because of peak overlap. After two rounds of structure calculation, the number of upper bound distance restraints

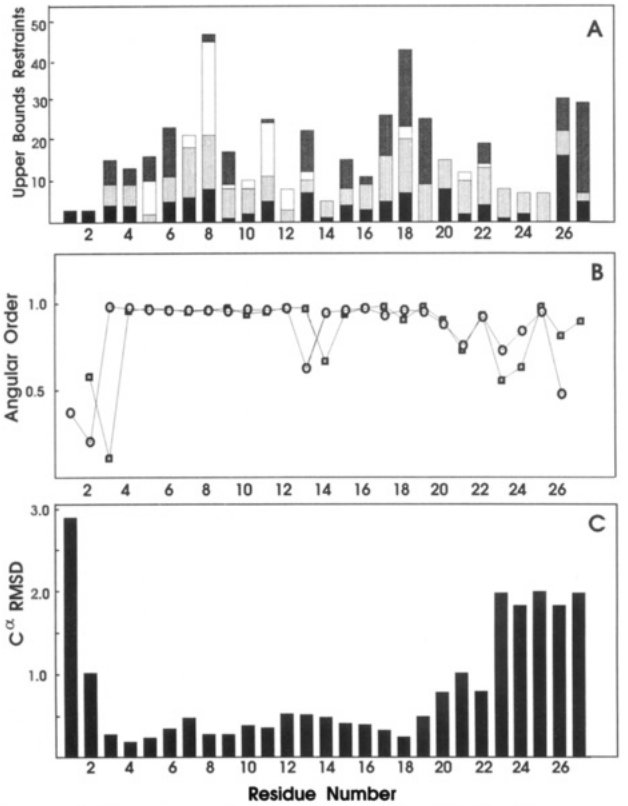

FIGURE 4: Parameters characterizing the final family of structures for ATX III, plotted as a function of residue number. (A) Distribution of upper bound restraints used in the final round of structure calculations. Long-range restraints (dark shading), defined as $|i - j| \geq 5$ for a restraint between residues i and j, medium-range (□), where $1 < |i - j| < 5$, sequential (light shading), and intraresidue (■) restraints are shown. Each restraint is counted twice, once for each proton involved, except in the case of intraresidue restraints, which are counted only once. (B) Angular order parameters for the backbone dihedral angles ϕ (▨) and ψ (○). (C) RMS differences from the mean structure for C^{α} atoms, calculated following superposition of the structures over the backbone heavy atoms (N, C^{α}, C) of residues 3–22.

was 291, of which 103 were intraresidue, 83 sequential, 32 medium-range ($1 < |i - j| < 5$), and 73 long-range (Figure 4A). This restraint list did not include distances fixed by the covalent geometry.

Two families of structures were calculated using X-PLOR version 3.1. The first family was based on the restraints described above and yielded 22 structures which met the criteria specified under Materials and Methods. These were then further refined following the inclusion of a set of 101 lower bound restraints reflecting the absence of NOEs. The set of 4600 lower bound restraints derived as described under Materials and Methods and used in the DSPACE calculations was not used in X-PLOR as the inclusion of such a large number of restraints increased the overall execution time by a factor of at least 5. The majority of these restraints was between pairs of protons that were already separated in the calculated structures by distances greater than the restraints and therefore served no useful purpose in the structure calculations. The set of 4600 lower bound restraints was filtered to leave only those restraints that had an effect on structure calculations. This was performed using in-house software which retained from the 4600 entries in the lower bounds list only those where the lower bound was greater than the minimum distance encountered over the initial family of 22 structures. This resulted in a set of 101 lower bound restraints.

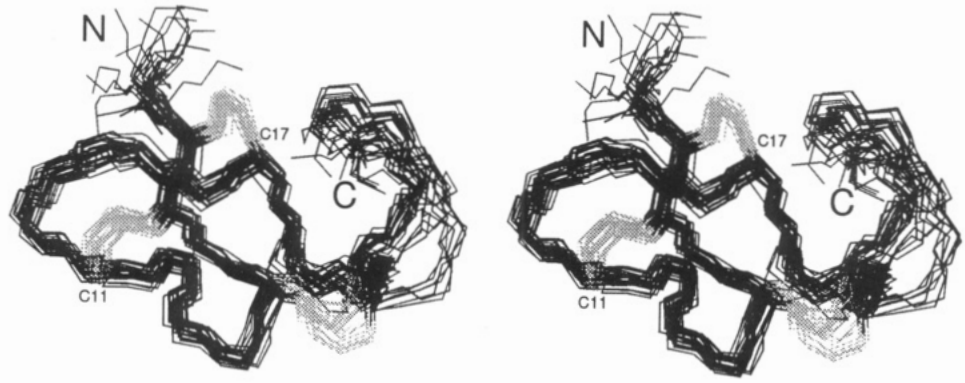

FIGURE 5: Stereoview of the 28 final structures of ATX III superimposed over the backbone heavy atoms (N, C^{α}, C) of residues 3–22. The three disulfide bonds are shown in lighter shading.

These lower bound restraints were used in conjunction with all other restraints to generate a new family of 80 structures, of which the best 17 were selected. In addition, the 22 structures calculated initially were refined using the lower bound restraints (with 2000 steps of simulated annealing cooling from 2000 K to 100 K, followed by 2000 steps of conjugate gradient minimization). Of these 22 structures, the best 11 were selected, giving a total of 28 final structures. Figure 4B shows the angular order parameters S (Hyberts et al., 1992; Pallaghy et al., 1993) for the backbone dihedral angles ϕ and ψ in these structures. Most residues are well-defined, with $S > 0.95$, although the N-terminus is disordered as a consequence of the lack of medium- and long-range NOEs to residues 1 and 2 (Figure 4A). The C^{α} RMS differences shown in Figure 4C mirror the angular order parameters, as expected, except for the five C-terminal residues, where the higher RMS differences reflect the poor definition around Ser23–Gly24, as discussed below.

The major effect on the structures of the inclusion of lower bound restraints was restriction of the backbone angles of residues 23–24. The retention factor for Ser23 was very low, and for this residue and Gly24 only intraresidue and sequential NOEs were observed, but lower bound restraints to the better defined residues at the C-terminus served to restrict the conformational space available to this part of the molecule, leading to better angular order parameters for residues 23–24 (e.g., values for the ϕ angles of residues 23 and 24 improved from 0.27 and 0.25, respectively, to 0.54 and 0.62). Because of the low retention factors associated with residues 1–2, lower bound restraints were not included for these residues, and their order parameters were not improved in the final set of structures. In general, the well-defined sections of the molecule were improved only slightly by inclusion of the lower bound restraints, with the RMS differences decreasing from 0.65 to 0.62 Å for the backbone heavy atoms and from 1.39 to 1.28 Å for all heavy atoms when the structures were superimposed over residues 3–22. Similar observations were made in the case of Sh I (Wilcox et al., 1993).

Structural Analysis. Stereoviews of the 28 final structures of ATX III superimposed over the backbone heavy atoms (N, C^{α}, C) of residues 3–22 are shown in Figure 5. Mean pairwise RMS differences over all residues were 1.32 ± 0.31 and 2.18 ± 0.38 Å for the backbone heavy atoms and all heavy atoms, respectively. Corresponding values for the well-defined bulk of the molecule, residues 3–22, were 0.62 ± 0.27 and 1.28 ± 0.29 Å, respectively. The RMS deviations from the experimental distance and dihedral restraints were 0.054 ± 0.002 Å (460 restraints) and 1.33 ± 0.17° (15 restraints), respectively, and the energy associated with the NOEs was 68.2 ± 5.3 kcal/mol.

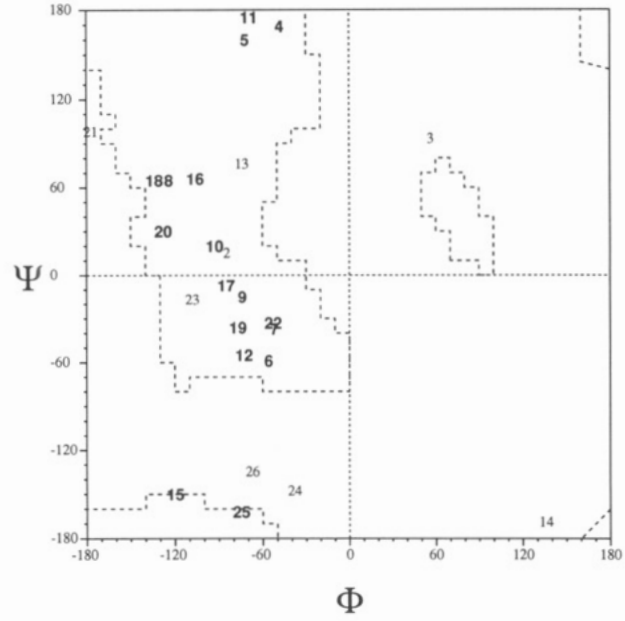

FIGURE 6: Ramachandran plot for the angular average of the 28 structures of ATX III. Boldface numbers denote residues with well-defined backbone dihedral angles ($S > 0.8$).

It is evident from Figures 4 and 5 that the two termini of the molecule are less well-defined than the rest. Residues 25–27 at the C-terminus are reasonably well-defined with respect to each other (Figure 4B), but the dipeptide unit Ser23–Gly24 is poorly defined, behaving rather like a hinge between residues 25–27 and the rest of the molecule. The flexibility and high degree of exposure of the C-terminal residues are consistent with the susceptibility of the C-terminus of ATX III to proteolysis to generate ATX IV (Beress, 1979). The N-terminus is also poorly defined, but in this case the lack of intraresidue and sequential NOEs (Figure 4A) suggests that Arg1 and Ser2 are probably mobile. As expected, there is a good correlation between how well-defined a given residue is in the final structures, as judged by its angular order parameters and RMS differences (Figure 4B,C), and the number of medium- and long-range NOEs it displays (Figure 4A).

A Ramachandran plot of the angular average of the final 28 structures is shown in Figure 6. All residues with well-defined backbone dihedral angles ($S > 0.8$) fall within the allowed regions. Cys3 has a positive ϕ angle for 15 of the 28 final structures although this residue is not in the well-defined category. Positive ϕ angles are found for 2% of non-glycine residues in the Protein Data Bank (Wilmot & Thornton, 1990). Ludvigsen and Poulsen (1992) noted that positive ϕ angles were associated with a strong intraresidue NH–C^{α}H NOE

Table 2: Location of Hydrogen Bonds and Slowly Exchanging Amide Protons in ATX III[a]

amide proton	hydrogen bond acceptor[b]	amide exchange rate[c]
Cys4	Gln15	S
Gly9	Cys6	I
Cys11	Trp8	S
Gly14	Pro12	S
Cys17	Gln15	S

[a] Hydrogen bonds were identified according to the criteria of Kabsch and Sander (1983). [b] Bonds to these acceptors were present in all 28 structures, except for that from Gly14 to Pro12, which was present in only 10 of the 28 structures. [c] Measured in ^2H_2O at pH 2.6 and 27 °C as described in Norton et al. (1993). Those designated slow (S) were observed in a TOCSY spectrum recorded on the exchanging sample, while those designated intermediate (I) were observed in 1D spectra recorded before the TOCSY but gave very weak cross-peaks in the 2D spectrum. Other residues with slowly exchanging NH protons are Tyr7, Trp8, Trp13, Gln15, Tyr18, Gly21, and Val27, while those of Glu20 and Ser23 are intermediate.

and a $^3J_{HNC^\alpha H}$ coupling constant of *ca.* 7Hz. For Cys3, a strong intraresidue NH–C$^\alpha$H NOE was observed, but a $^3J_{HNC^\alpha H}$ of *ca.* 7Hz could not be confirmed due to spectral overlap.

Description of the Structure. The overall fold of ATX III is evident in Figure 5, where the backbone atoms of the best 28 structures are superimposed. The molecule appears to lack any regular secondary structure in the form of β-sheet or α-helix, consisting instead of a series of reverse turns. Consideration of the backbone ϕ/ψ angles in conjunction with the locations of hydrogen-bonded amides, which are summarized in Table 2, leads to the identification of four turns. The first is a distorted type I turn involving residues 6–9, with average dihedral angles $\phi_2 = -52°$, $\psi_2 = -38°$ and $\phi_3 = -124°$, $\psi_3 = 66°$ and a hydrogen bond from Gly9 to Cys6. The second is a type I turn involving residues 8–11, with average dihedral angles $\phi_2 = -74°$, $\psi_2 = -16°$ and $\phi_3 = -96°$, $\psi_3 = 20°$ and a hydrogen bond from Cys11 to Trp8. The remaining two turns are inverse γ turns involving residues 12–14 ($\phi_2 = -75°$, $\psi_2 = 77°$) and 15–17 ($\phi_2 = -109°$, $\psi_2 = 66°$), each having an i+2 to i hydrogen bond (Table 2). The presence of a succession of turns between residues 6 and 17 suggests the possibility of a helical structure, but there are too many distortions associated with changes in chain direction for this description to be appropriate. Two other chain reversals are evident from inspection of the structures, involving residues 18–21 and 21–25, respectively. The first of these has ϕ and ψ angles consistent with a distorted type I turn, but there is no hydrogen bond from Gly21 to Tyr18. It is interesting to note, however, that the NH of Gly21 was found to be slowly exchanging (Norton et al., 1993).

Figure 7 shows the region of the structures encompassing the five surface-exposed residues most affected by aggregation. The positions of Pro5, Trp8, Pro12, and Trp13 are well-defined due to the large number of NOEs to these residues, and they form a hydrophobic surface on the molecule which must constitute part of the site of aggregation. The side chain of Tyr7 is rather poorly defined, as there are no long-range and only a few medium-range NOEs to its ring protons. While it is located on the surface of the molecule and is therefore potentially mobile, its aromatic ring protons display the most concentration-dependent chemical shifts, implying that it forms part of the aggregation surface and may therefore be motionally restricted in the aggregate. The lack of NOEs to its aromatic protons serves to emphasize that intermolecular interactions in the aggregate do not give rise to observable NOEs, even when chemical shifts are significantly affected. Cys11 is the other residue with chemical shifts strongly affected by aggregation. This residue appears to be buried in the structures. Resonances from its C$^\alpha$H proton and one C$^\beta$H proton are shifted upfield from their corresponding values in unstructured peptides (Wüthrich, 1986) by approximately 2.0 and 2.8 ppm, respectively, at the 5 mM concentration. The reason for this upfield shift is apparent from the structures, as Cys11 is situated near the indole rings of Trp8 and Trp13, and likely to be strongly affected by the ring currents of these residues (Wüthrich, 1986). It follows that the marked concentration dependence of its chemical shifts may reflect alterations in the positions of these aromatic rings rather than direct intermolecular interactions involving Cys11. One of the C$^\beta$H resonances of Pro5 is also shifted upfield by 1.4 ppm and is also very close to the Trp residues.

Figure 8 shows the locations of all side chains in the individual structure of ATX III which is closest to the average over all 28. The van der Waals surfaces of the five surface side chains affected by aggregation (Pro5, Tyr7, Trp8, Pro12, and Trp13) are shaded, and the locations of the five charged groups are shown in boldface. The two positively charged groups of Arg1 lie relatively close to the hydrophobic patch in this view, but it must be borne in mind that the position of Arg1 is poorly defined (Figure 4). The two carboxyl groups and the ϵ-ammonium of Lys26 are on the opposite face of the molecule, well separated from the hydrophobic patch.

The environment of Tyr18 in the structure (Figure 8) was somewhat unexpected on the basis of previous observations (Norton et al., 1993). The chemical shifts of its aromatic protons are very close to those for tyrosine in a random coil and do not vary with concentration or pH until the phenolic group titrates. Moreover, the phenolic pK_a is essentially identical to that in small peptides. It was therefore expected that Tyr18 would be located on the surface of the molecule and participate in few interresidue interactions, but in fact it displays a large number of NOEs (Figure 3) and is well-defined in the final structures (Figure 4), where it sits in a cavity in close proximity to several other residues. Its phenolic group is exposed to the solvent, which is consistent with its pH titration behavior, and the absence of other aromatic residues from its immediate environment is consistent with its unperturbed chemical shifts. Nevertheless, it is not the fully exposed surface residue that might have been expected.

The conformations of the 3–17 and 4–11 disulfide bonds in ATX III are very well-defined, as shown in Figure 5, while that of the 6–22 bond is more variable. Using the categories of disulfide bond conformation proposed by Srinivasan et al. (1990), the 3–17 bond is a distorted type 1, 4–11 a type 2, and 6–22 a type 7. The 4–11 bond is completely inaccessible to solvent, and the other two bonds have low accessibility, with the 6–22 bond being the most exposed. Overall, the structure is reasonably compact, with a total surface area of 1626 Å^2 and a contact area of 567 Å^2. Corresponding values for ω-conotoxin GVIA, which has the same number of residues and disulfide bonds but a 3% higher molecular mass, are 1866 Å^2 and 641 Å^2, respectively (Pallaghy et al., 1993).

As described above, there are five backbone amide protons involved in hydrogen bonds associated with reverse turns. All of these were identified as having slow or intermediate exchange rates by Norton et al. (1993), but there are also a number of other slowly exchanging amides which do not participate in clearly defined hydrogen bonds in our structures. The amide of Trp8 hydrogen bonds with the carbonyl of Pro5 in 4 of the 28 structures and that of Gln15 interacts with Ser2 in 5, but hydrogen bonds are not observed for the amides of Tyr7, Trp13, Tyr18, Gly21, and Val27. The amides of Trp13

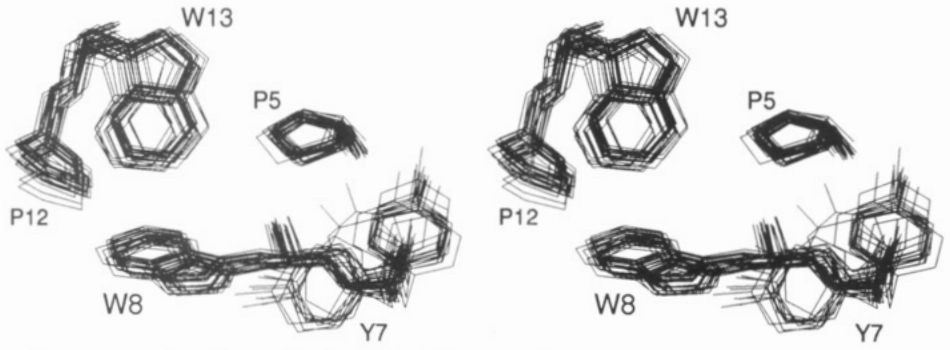

FIGURE 7: Stereoview of the 5 exposed residues with chemical shifts most affected by aggregation (*cf.* Figure 1) in the 28 final structures of ATX III superimposed over the backbone heavy atoms (N, C^{α}, C) of residues 3–22. Side chains are shown for all residues, and connecting backbone for residues 7–8 and 12–13.

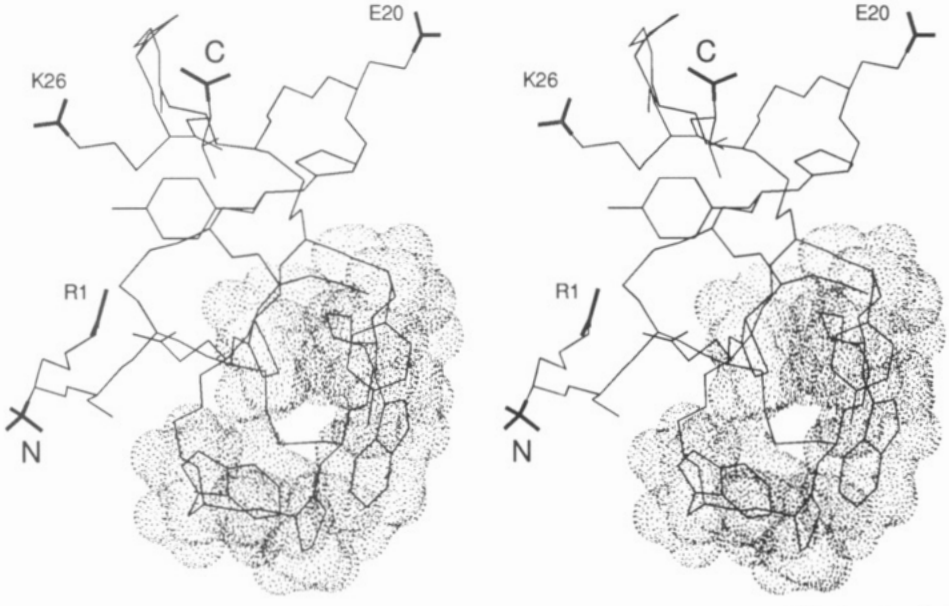

FIGURE 8: Stereoview of the individual structure of ATX III which is closest to the average over all 28 showing the backbone and all side chains. The van der Waals surfaces for residues 5, 7, 8, 12, and 13 are shaded, while the five charged groups in the molecule are shown in boldface.

and Tyr18 are not accessible to solvent in any of the structures, and those of Tyr7 and Val27 are accessible in only a few. It is possible that one or more of these amides forms hydrogen bonds with bound water molecules. The amide of Gly21 is accessible to solvent in 60% of the structures, and it may be that structures in which it is more buried and perhaps able to form a hydrogen bond to Tyr18 to create a type 1 turn (see above) are more representative of the local structure in this region of the molecule, or that its exchange rate is affected by aggregation. In bovine pancreatic trypsin inhibitor, for example, four amides were slowly exchanging in concentrated solution but rapidly exchanging in dilute solution (Pardi et al., 1983).

DISCUSSION

In this paper, we have described the three-dimensional structure in aqueous solution of neurotoxin III from the sea anemone *Anemonia sulcata*. The structure is generally well-defined for all residues except the N-terminal residues Arg1, Ser2, and Cys3 and a hinge region close to the C-terminus at Ser23 and Gly24. The disulfide pairings of the six half-cystine residues were unknown and had to be determined in this study from analysis of a family of structures generated without disulfide bonds formed. The pairings follow a 1–5/2–4/3–6 pattern, which is in fact the same as that of the long sea anemone toxins. This may be fortuitous, but it suggests that ATX III is related to the long toxins by a series of insertions and deletions between conserved cysteine residues. The magnitude of these changes, however, is such that the three-dimensional structures bear little resemblance to one another.

Both in determining the disulfide pairings and in better defining certain regions of the final structures, we made use of lower bound restraints derived from the absence of NOE cross-peaks in the NOESY spectrum. While there are many examples of the use of lower bound restraints in the literature (de Vlieg et al., 1986; Kim & Reid, 1992; Wilcox et al., 1993; Pallaghy et al., 1993), considerable caution is still called for in their application because of the possibility of reductions in NOE intensities due to factors such as internal motion, spectral artifacts, and solvent suppression. The procedure adopted in this work involves a progressive reduction, on the basis of measured intensities for other NOEs involving the contributing protons, in the value of a lower bound distance inferred from the absence of an NOE. This is quantified in the form of a retention factor for each proton in the molecule. We believe that the application of this approach permits lower bound restraints greater than 1.8 Å to be employed with greater confidence in structure determinations. From our experience in this study and previously in refinement of the structure of Sh I (Wilcox et al., 1993), it appears that the use of lower bound restraints has relatively little effect on the well-defined regions of the molecule but can lead to useful improvements in regions that are poorly defined by the upper bound restraints.

Nevertheless, if even slight improvements in the well-defined regions of a structure can be achieved with a minimum of effort through automation of the procedures involved in measuring non-NOEs, applying retention factors, and selecting nonredundant lower bound restraints, then the use of such restraints may be worthwhile. Lower bound restraints are also potentially helpful in applications such as the definition of disulfide bond pairings where there are several cysteine residues close to one another in the sequence and there may be numerous NOEs among nonbonded half-cystines. In this instance, the lower bound restraints are useful in restricting the conformational space available to the side chains, making it easier to identify the correct pairings. The retention factors calculated during the course of deriving lower bound restraints can also provide a crude indicator of the role of internal motions in poorly defined regions of a molecule. Thus, if retention factors calculated from intraresidue NOE intensities are low, then internal motion may be present (although other explanations are possible), but if residues that are poorly defined in a structure because of a lack of medium- or long-range NOEs have retention factors close to 1, this may indicate that their poor definition is due to a lack of local structural constraints rather than simply fast internal motion. Relaxation time measurements provide the best means of quantifying internal motions.

The self-association of ATX III at concentrations used to acquire 2D NMR spectra dictated that precautions be taken to exclude intermolecular NOEs from the NMR restraint set. In fact, it appeared that there were no significant NOEs of this type, perhaps indicating that the association is a rather weak one despite its obvious effects on the chemical shifts of certain residues. These observations may be yet another manifestation of the greater sensitivity to local perturbations of chemical shifts compared with NOEs. For example, in the type 2 sea anemone toxin *Heteractis macrodactylus* toxin III, the presence of a tyrosine at position 11 in place of an asparagine caused chemical shift changes of up to 0.3 ppm in several resonances and yet the aromatic ring of Tyr11 showed no long-range NOEs at all (Hinds & Norton, 1993).

The propensity of ATX III to aggregate reflects at least partly the presence of a number of hydrophobic side chains on its molecular surface. This is particularly marked in the region of the six residues with the most concentration-dependent chemical shifts, Pro5, Tyr7, Trp8, Cys11, Pro12, and Trp13. Except for Cys11, all of these side chains are exposed (Figure 8) and are likely to form part of the aggregation surface. As a consequence, it is possible that the orientations of some of these side chains in the structures presented here are affected by intermolecular interactions even though these interactions are not strong enough to generate intermolecular NOEs. As noted above, the presence of three aromatic residues in this region no doubt contributes to the significant changes in chemical shift as a function of concentration. Other regions of the molecule are probably also involved in aggregation, including possibly the C-terminal carboxyl group. Detailed analytical ultracentrifugation experiments are in progress to further characteize this self-association and to examine its pH, salt, and temperature dependence. Preliminary results indicate that the molecule is predominantly monomeric at concentrations of 0.1 mM or less,[3] suggesting that the biologically active species is the monomer.

The hydrophobic patch on the surface of ATX III may be important functionally. Fontecilla-Camps et al. (1988) have noted that the α-scorpion toxin *Androctonus australis* Hector II has a "conserved hydrophobic" surface consisting of a number of aliphatic and aromatic residues as well as some positively charged residues, which they proposed to be part of the sodium channel binding surface. The type 1 sea anemone polypeptides AP-A and ATX Ia have two Trp residues in close spatial proximity (Gooley et al., 1986; Torda et al., 1988; Widmer et al., 1989), both of which are at least partially exposed to solvent (Norton et al., 1986). The crude similarity with ATX III, where two Trp residues are also exposed on the surface, is obvious, but a more detailed comparison of the surfaces is required to assess the potential significance of this observation. In PaTx, the only other short anemone toxin characterized to date, five of the six residues in the hydrophobic region of ATX III are conserved, the exception being Trp8, which is replaced by Thr (Nishida et al., 1985; Norton, 1991). This is consistent with a role for this region in maintenance of the tertiary structure, if not also in sodium channel binding. Chemical modification studies described below lend support to this proposition.

A common feature of both classes of long sea anemone toxins is a loop of about 10 residues which commences around residues 7–8 and is less well-defined than the bulk of the structure in all of the NMR-based structures determined so far (Torda et al., 1988; Widmer et al., 1989; Fogh et al., 1990; Wilcox et al., 1993). Carboxyl-containing residues near the start of this loop are essential for activity, and it contains several residues which are conserved in all type 1 and 2 toxins, such as Gly9, Pro10, and Arg13 (Norton, 1991). Furthermore, selective proteolysis of this loop at Arg13 inactivates AP-A (Gould et al., 1990) and Sh I (Monks et al., 1994). ATX III does not have an equivalent loop, but the N-terminal Arg in ATX III is poorly defined, as is the conserved Arg at position 13 in the long toxins. In AP-A, the guanidino group of Arg14 is separated from the essential carboxyl groups of Asp7 and -9 by distances of 10–20 Å, while in ATX III the corresponding distances between Arg1, Glu20, and Val27 are a few angstroms longer. Interestingly, the distances between the carboxyl groups themselves are very similar in the two molecules, at 8–9 Å.

Beress (1979) carried out a number of chemical modifications on ATX III to probe its structure–function relationships. Unfortunately, the products of these modifications were usually not separated chromatographically or characterized chemically, but the results point to some residues that may be essential for activity. As might be expected, reduction of all three disulfide bonds with dithiothreitol destroyed activity, but there was also an indication that reduction of just one had the same effect. In our structures, the most exposed disulfide is 6–22. Acetylation of the N-terminal ammonium group reduced the toxicity by 70% in ATX III. In ATX IV, which lacks the C-terminal Lys and Val residues and has only 30% of the activity of ATX III, acetylation further reduced the activity to 8%. This suggests that the N-terminal ammonium is required for full activity and that either a C-terminal side chain or the position of the C-terminal carboxyl is also important. Nitration of the two tyrosines with tetranitromethane reduced the activity to only 5%, while reaction of the tryptophans with 2-hydroxy-5-nitrobenzyl bromide reduced the activity to 70 and 20%, respectively, when 0.8 and 1.5 residues were modified (as measured spectrophotometrically). Thus, it seems that one or both tyrosines and one of the tryptophans are important for activity, consistent with the idea that the hydrophobic patch described above has a role in sodium channel binding. By analogy with other toxic polypeptides that affect ion channel function, it is likely that the sodium channel binding surface of ATX III involves a number of side chains, several of which can be modified without

complete loss of biological activity. A systematic investigation of residues thought to be essential for activity is now required using peptide synthesis, which should be straightforward for ATX III.

Finally, it should be noted that ATX III is the smallest of the sea anemone-derived sodium channel binding toxins for which a high-resolution structure has been determined. Although it is not active on the sodium channel of the mammalian heart, it appears to act at a similar site and by a similar mechanism on the crustacean nerve sodium channel, suggesting that it might be possible to engineer mammalian cardiac activity into ATX III. Given that it is approximately half the size of the long toxins, this may offer a useful alternative route to defining the minimal active structural element for cardiac stimulatory activity.

ACKNOWLEDGMENTS

We thank Laszlo Beress for the sample of ATX III, David Craik for the program COUPLING.ERIK, David Smith for the program SSTRUC, Richard Ford for assistance with computing, and Paul Pallaghy and Gavin Wilcox for many useful discussions. The programs described in this paper for measuring and applying lower bound restraints will be made available on request from the authors.

REFERENCES

Adler, M., Carter, P., Lazarus, R. A., & Wagner, G. (1993) *Biochemistry 32*, 282–289.
Beress, L. (1979) Habilitationschrift, Institut für Meereskunde an der Christian-Albrechts Universität, Kiel.
Beress, L. (1982) *Pure Appl. Chem. 54*, 1981–1994.
Beress, L., Beress, R., & Wunderer, G. (1975) *FEBS Lett. 50*, 311–314.
Blake, C. C. F., Ghosh, M., Harlos, K., Avezoux, A., & Anthony, C. (1994) *Nat. Struct. Biol. 1*, 102–105.
Brünger, A. T. (1992) *X-PLOR Version 3.1. A System for X-ray Crystallography and NMR*, Yale University, New Haven, CT.
Catterall, W. A. (1988) *Science 242*, 50–61.
Catterall, W. A., & Beress, L. (1978) *J. Biol. Chem. 253*, 7393–7396.
Clore, G. M., Gronenborn, A. M., Carlson, G., & Meyer, E. F. (1986) *J. Mol. Biol. 190*, 259–267.
Cooke, R. M., Carter, B. G., Murray-Rust, P., Hartshorn, M. J., Herzyk, P., & Hubbard, R. E. (1992) *Protein Eng. 5*, 473–477.
de Vlieg, J., Boelens, R., Scheek, R. M., Kaptein, R., & van Gunsteren, W. F. (1986) *Isr. J. Chem. 27*, 181–188.
Fontecilla-Camps, J. C., Habersetzer-Rochat, C., & Rochat, H. (1988) *Proc. Natl. Acad. Sci. U.S.A. 85*, 7443–7447.
Fogh, R. H., Kem, W. R., & Norton, R. S. (1990) *J. Biol. Chem. 265*, 13016–13028.
Gooley, P. R., Blunt, J. W., Beress, L., Norton, T. R., & Norton, R. S. (1986) *J. Biol. Chem. 261*, 1536–1542.
Gould, A. R., Mabbutt, B. C., & Norton, R. S. (1990) *Eur. J. Biochem. 189*, 145–153.
Griesinger, C., Sorensen, O. W., & Ernst, R. R. (1987) *J. Magn. Reson. 75*, 474–492.
Heitz, A., Chiche, L., Le Nguyen, D., & Castro, B. (1989) *Biochemistry 28*, 2392–2398.
Hinds, M. G., & Norton, R. S. (1993) *J. Protein Chem. 12*, 371–378.
Hyberts, S. G., Märki, W., & Wagner, G. (1987) *Eur. J. Biochem. 164*, 625–635.
Hyberts, S. G., Goldberg, M. S., Havel, T. F., & Wagner, G. (1992) *Protein Sci. 1*, 736–751.
Jeener, J., Meier, B. H., Bachmann, P., & Ernst, R. R. (1979) *J. Chem. Phys. 71*, 4546–4553.
Johnson, B. A., & Sugg, E. E. (1992) *Biochemistry 31*, 8151–8159.
Kabsch, W., & Sander, C. (1983) *Biopolymers 22*, 2577–2637.
Kem, W. R. (1988) in *The Biology of Nematocysts* (Hessinger, D., & Lenhoff, H., Eds.) pp 375–405, Academic Press, New York.
Kim, S.-G., & Reid, B. R. (1992) *J. Magn. Reson. 100*, 382–390.
Klaus, W., Broger, C., Gerber, P., & Senn, H. (1993) *J. Mol. Biol. 232*, 897–906.
Llewellyn, L. E., & Norton, R. S. (1991) *Biochem. Int. 24*, 937–946.
Ludvigsen, S., & Poulsen, F. M. (1992) *J. Biomol. NMR 2*, 227–233.
Macura, S., Huang, Y., Suter, D., & Ernst, R. R. (1981) *J. Magn. Reson. 43*, 259–281.
Manoleras, N., & Norton, R. S. (1992) *J. Biomol. NMR 2*, 485–494.
Marion, D., & Wüthrich, K. (1983) *Biochem. Biophys. Res. Commun. 113*, 967–974.
Metzler, W. J., Valentine, K., Roebber, M., Friedrichs, M. S., Marsh, D. G., & Mueller, L. (1992) *Biochemistry 31*, 5117–5127.
Monks, S. A., Gould, A. R., Lumley, P. E., Alewood, P. F., Kem, W. R., Goss, N. H., & Norton, R. S. (1994) *Biochim. Biophys. Acta* (in press).
Neuhaus, D., & Williamson, M. P. (1989) *The Nuclear Overhauser Effect in Structural and Conformational Analysis*, pp 358–359, VCH Publishers, New York.
Neuhaus, D., Wagner, G., Vasak, M., Kagi, H. R., & Wüthrich, K. (1985) *Eur. J. Biochem. 151*, 257–273.
Nishida, S., Fujita, S., Warashina, A., Satake, M., & Tamiya, N. (1985) *Eur. J. Biochem. 150*, 171–173.
Norton, R. S. (1991) *Toxicon 29*, 1051–1084.
Norton, R. S., Beress, L., Stob, S., Boelens, R., & Kaptein, R. (1986) *Eur. J. Biochem. 157*, 343–346.
Norton, R. S., Cross, K., Braach-Maksvytis, V., & Wachter, E. (1993) *Biochem. J. 293*, 545–551.
Norton, T. R. (1981) *Fed. Proc., Fed. Am. Soc. Exp. Biol. 40*, 21–25.
Pallaghy, P. K., Duggan, B. M., Pennington, M. W., & Norton, R. S. (1993) *J. Mol. Biol. 234*, 405–420.
Pardi, A., Wagner, G., & Wüthrich, K. (1983) *Eur. J. Biochem. 137*, 445–454.
Pardi, A., Billeter, M., & Wüthrich, K. (1984) *J. Mol. Biol. 180*, 741–751.
Rance, M., Sorensen, O. W., Bodenhausen, G., Wagner, G., Ernst, R. R., & Wüthrich, K. (1983) *Biochem. Biophys. Res. Commun. 117*, 479–485.
Renaud, J.-F., Fosset, M., Schweitz, H., & Lazdunski, M. (1986) *Eur. J. Pharmacol. 120*, 161–170.
Smith, L. J., Sutcliffe, M. J., Redfield, C., & Dobson, C. M. (1991) *Biochemistry 30*, 986–996.
Srinivasan, N., Sowdhamini, R., Ramakrishnan, C., & Balaram, P. (1990) *Int. J. Pept. Protein Res. 36*, 147–155.
Torda, A. E., Mabbutt, B. C., van Gunsteren, W. F., & Norton, R. S. (1988) *FEBS Lett. 239*, 266–270.
Wagner, G., Braun, W., Havel, T. F., Schaumann, T., Gō, N., & Wüthrich, K. (1987) *J. Mol. Biol. 196*, 611–639.
Warashina, A., Jiang, Z.-Y., & Ogura, T. (1988) *Eur. J. Physiol. 411*, 88–93.
Weber, P. L., Morrison, R., & Hare, D. (1988) *J. Mol. Biol. 204*, 483–487.
Widmer, H., Billeter, M., & Wüthrich, K. (1989) *Proteins: Struct., Funct., Genet. 6*, 357–371.
Wilcox, G. R., Fogh, R. H., & Norton, R. S. (1993) *J. Biol. Chem. 268*, 24707–24719.
Williamson, M. P., Havel, T. F., & Wüthrich, K. (1985) *J. Mol. Biol. 182*, 295–315.
Wilmot, C. M., & Thornton, J. M. (1990) *Protein Eng. 3*, 479–493.
Wüthrich, K. (1986) *NMR of Proteins and Nucleic Acids*, Wiley, New York.